A unified solute diffusion model for columnar and equiaxed dendritic alloy solidification

C. Y. Wang and C. Beckermann

Department of Mechanical Engineering, The University of Iowa, Iowa City, IA 52242 (USA)

(Received December 11, 1992; in revised form April 7, 1993)

Abstract

A unified solute diffusion model is proposed for columnar and equiaxed dendritic alloy solidification, in which nucleation, growth kinetics and dendrite morphology are taken into account. Various applications to a uniformly solidified system are demonstrated, with emphasis on three special cases: complete solute mixing in the liquid, columnar growth with significant dendrite tip undercooling, and equiaxed dendritic growth. Theoretical predictions of microsegregation, eutectic fractions and cooling curves are compared with a number of previous theoretical and experimental results, and good agreement is found.

1. Introduction

The prediction of microstructure formation during dendritic alloy solidification is of great importance for the evaluation of properties and control of the quality of castings. To this aim, a micro-macroscopic modeling approach [1] has been proposed, in which a macroscopic model calculates the temperature field within a casting, while microscopic models predict microstructural features based on the fundamental mechanisms of nucleation and growth of dendrites. A key component in this approach is the solute diffusion model which provides the evolution of the local solid fraction for use in the macroscopic energy equation, and thus provides a major linkage between the microscopic and macroscopic aspects of solidification.

As reviewed by Rappaz [1], previous solute diffusion models for dendritic solidification can be classified as follows: (1) equilibrium models which do not consider nucleation and undercooling; (2) models for columnar growth which incorporate dendrite tip undercooling; (3) models for equiaxed growth focusing on coupling the growth kinetics of dendrite tips to the evolution of an equiaxed grain.

The first category of solute diffusion models essentially aims at investigating the effect of back diffusion in the solid, while the liquid is assumed to be solutally well mixed [2, 3]. Three basic analytical equations have been obtained depending on the extent of solute diffusion in the solid: (1) the Lever rule where complete solute mixing is also assumed in the solid [4], (2) the Scheil equation where solute diffusion in the solid is absent [4], and (3) the Brody–Flemings model [5] (later modified by Clyne and Kurz [6]) for finite rate diffusion in the solid. More recently, Ohnaka [7] derived a simple expression for an improved estimate of microsegregation using the integral method. Kobayashi [8] obtained an exact solution to the solute redistribution problem. Available in the literature are also a number of numerical models that can handle cases with variable properties and dendrite arm coarsening [2, 3, 9–11]. However, none of the above models account for dendrite tip undercooling and are thus expected to be inapplicable at medium and high cooling rates.

During near-rapid and rapid solidification processes as described by Flemings [12], dendrite tip undercooling at the columnar front can become sufficiently large to affect the relationship between the solid fraction and temperature. Several authors have therefore attempted to incorporate the growth kinetics of the dendrite tip in modeling columnar growth. Assuming no back diffusion in the solid, Flood and Hunt [13] used the Scheil equation truncated at the tip temperature; however, their model suffers from the shortcoming that solute is not conserved [1]. More recently, Giovanola and Kurz [14] proposed an empirical approach to arrive at an $\varepsilon_s(T, V_t)$ relation using the Scheil equation and the Kurz, Giovanola and Trivedi model [15] of dendrite tip growth. Again, back diffusion in the solid is neglected. The model divides the mushy zone into two regions, with non-equilibrium growth allowed only in the tip region and a state of complete solute mixing in the

0921-5093/93/$6.00

liquid assumed in the other region. Then, a curve-fitted polynomial and the Scheil equation are utilized for the solid fraction profiles in the two regions respectively. Owing to the fact that the model conserves solute everywhere, it produces the best approximation at present, as commented on by Rappaz [1].

In order to predict microsegregation at both low and high cooling rates, the combined effects of back diffusion and dendrite tip undercooling need to be considered. Although Solari and Biloni [16] include both effects, their analysis is obsolete because it relies on the Brody–Flemings derivation [5] and the growth equation of Burden and Hunt for the dendrite tip [17]; the former was modified in ref. 6 and the latter is known to be inapplicable at high cooling rates [1]. More recently, Exner *et al.* [18] reported a set of numerical results for the eutectic fraction for various Al–Cu alloys solidified under a wide range of cooling rates. The details of their model [19], along with another study by Voller and Sundarraj [20] dealing with microsegregation in the presence of undercooling, became available after submission of the present paper. By solving numerically a partial differential equation for solute diffusion and incorporating both the dendrite tip and eutectic undercoolings, Roosz and Exner [19] and Voller and Sundarraj [20] independently succeeded in predicting the eutectic fraction over a wide range of cooling rates, and achieved good agreement with Sarreal and Abbaschian's experiments [21].

The solute diffusion processes occurring in equiaxed dendritic growth are even more difficult to model, mainly because an equiaxed dendrite is not fully solid. Several approaches have been reported in the literature. Dustin and Kurz [22] presumed that a mushy grain has a constant internal solid fraction. Recently, Rappaz and Thevoz [23, 24] took full account of nucleation and growth kinetics, and introduced a spherical grain envelope which separates the interdendritic from the extradendritic liquids. The interdendritic liquid is assumed to be solutally well mixed, and the dynamics of the envelope are determined by the growth kinetics of the dendrite tips. Both numerical and analytical versions of this solute diffusion model were formulated.

The objective of the present paper is to present a unified solute diffusion model for both columnar and equiaxed dendritic growth, which incorporates descriptions of nucleation, growth kinetics and dendrite morphology. The model is a simplified version of a recently developed multiphase micro-macroscopic model [25], which was derived using the so-called volume averaging technique. The resulting solute diffusion model consists of a set of ordinary differential equations and is coupled to a characteristic solidification equation. Various applications of the model are demonstrated, and the model predictions are compared with a number of theoretical and experimental results available in the literature.

2. Model and analysis

2.1. Solute diffusion equations

Consider a volume element containing either columnar or equiaxed dendrites, as shown in Figs. 1(a) and

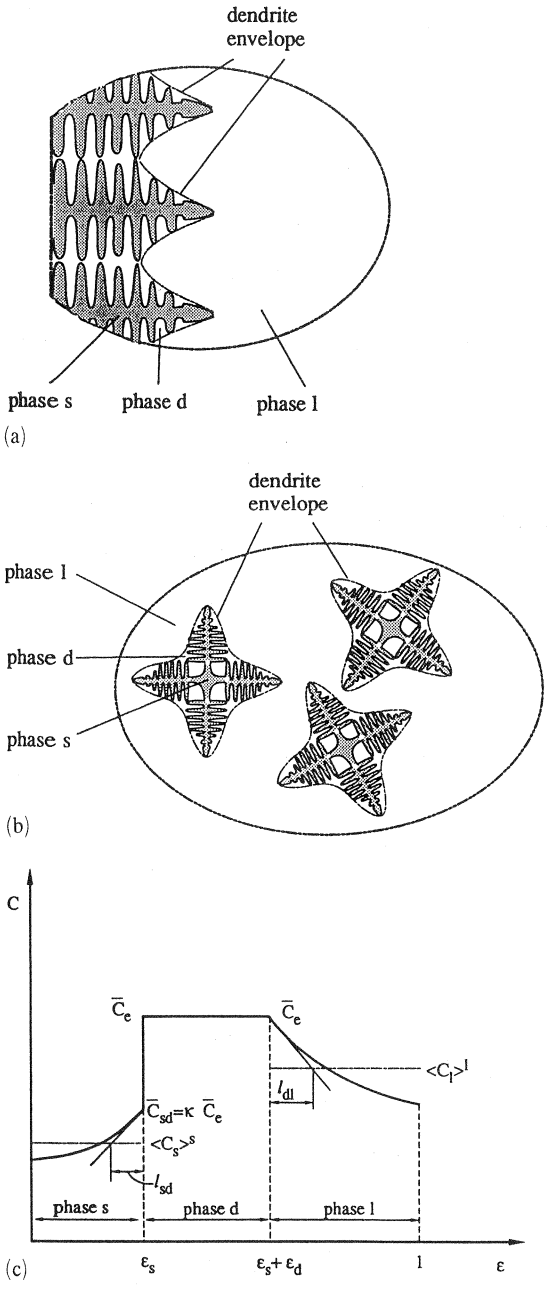

Fig. 1. Schematic diagram of the physical model: (a) columnar dendritic growth, (b) equiaxed dendritic growth, and (c) solute profiles and diffusion lengths in the various phases.

1(b). The volume is assumed to be at a uniform temperature and is occupied by three quiescent phases: the solid (s), the interdendritic liquid (d), and the extradendritic liquid (l). The two liquid phases are associated with different interfacial length scales and possess different transport behaviors. Complete solute mixing is nearly true in the interdendritic liquid because of the large area of the solid–liquid interface, whereas substantial undercooling may exist in the extradendritic liquid [1, 3, 23]. This is shown schematically in Fig. 1(c). The dendrite envelope is defined as the interface separating the two liquid phases, and its movement is governed by the growth kinetics of the dendrite tips. The reader is referred to ref. 25 for a more thorough discussion of this multiphase approach. Assuming that the densities of the solid and liquid phases are constant and equal, one can derive the following set of differential equations governing solute diffusion in the present three-phase system (see Appendix A for nomenclature):

envelope motion

$$\frac{\mathrm{d}}{\mathrm{d}t}(\varepsilon_\mathrm{s}+\varepsilon_\mathrm{d})=S_\mathrm{e}\bar{w}_\mathrm{ne}=\frac{S_\mathrm{e}D_\mathrm{l}m(\kappa-1)\bar{C}_\mathrm{e}}{\pi^2\Gamma}[\mathrm{Iv}^{-1}(\Omega)]^2 \tag{1}$$

solute balance of phase s

$$\frac{\mathrm{d}(\varepsilon_\mathrm{s}\langle C_\mathrm{s}\rangle^\mathrm{s})}{\mathrm{d}t}=\bar{C}_\mathrm{sd}\frac{\mathrm{d}\varepsilon_\mathrm{s}}{\mathrm{d}t}+\frac{S_\mathrm{s}D_\mathrm{s}}{l_\mathrm{sd}}(\bar{C}_\mathrm{sd}-\langle C_\mathrm{s}\rangle^\mathrm{s}) \tag{2}$$

solute balance of phase d

$$\frac{\mathrm{d}(\varepsilon_\mathrm{d}\bar{C}_\mathrm{e})}{\mathrm{d}t}=(1-\kappa)\bar{C}_\mathrm{e}\frac{\mathrm{d}\varepsilon_\mathrm{s}}{\mathrm{d}t}+\bar{C}_\mathrm{e}\frac{\mathrm{d}\varepsilon_\mathrm{d}}{\mathrm{d}t}-\frac{S_\mathrm{e}D_\mathrm{l}}{l_\mathrm{ld}}(\bar{C}_\mathrm{e}-\langle C_\mathrm{l}\rangle^\mathrm{l})-\frac{S_\mathrm{s}D_\mathrm{s}}{l_\mathrm{sd}}(\bar{C}_\mathrm{sd}-\langle C_\mathrm{s}\rangle^\mathrm{s}) \tag{3}$$

solute balance of phase l

$$\frac{\mathrm{d}[\varepsilon_\mathrm{l}\langle C_\mathrm{l}\rangle^\mathrm{l}]}{\mathrm{d}t}=\bar{C}_\mathrm{e}\frac{\mathrm{d}\varepsilon_\mathrm{l}}{\mathrm{d}t}+\frac{S_\mathrm{e}D_\mathrm{l}}{l_\mathrm{ld}}(\bar{C}_\mathrm{e}-\langle C_\mathrm{l}\rangle^\mathrm{l}) \tag{4}$$

This set of equations has been rigorously derived by the volume averaging technique [25]. Apart from the physical properties which are explained in Appendix A, several notations are clarified here. First, the term $\langle C_k\rangle^k$ denotes the volume averaged intrinsic concentration of a phase k, with $\langle\cdot\rangle$ being the conventional symbol used in the volume averaging method. Physically, the term $\langle C_k\rangle^k$ is nothing else but the mean concentration in a phase. However, the overbar denotes an interfacial average, so that the symbol $\bar{C}_\mathrm{e}$ stands for the mean concentration of the envelope. Because the interdendritic liquid is assumed to be solutally well mixed, $\bar{C}_\mathrm{e}$ is also equal to the equilibrium liquid concentration at the solid–liquid interface and is related to the local temperature by the liquidus line of the phase diagram. The concentration on the solid side $\bar{C}_\mathrm{sd}$ is accordingly given by

$$\bar{C}_\mathrm{sd}=\kappa\bar{C}_\mathrm{e} \tag{5}$$

Second, ε_k is the volume fraction of a phase k. Third, S designates the area concentration of an interface, which is defined as the ratio of the interfacial area to the volume of the volume element. Therefore, S represents the inverse of a microscopic length scale. Note that the area concentration of the solid–liquid interface S_s in dendritic growth is typically much larger than the envelope area concentration S_e. Last, l_sd and l_ld denote the solid and liquid diffusion lengths respectively. Their physical meanings are illustrated schematically in Fig. 1(c).

Equations (1)–(4) all have simple physical interpretations. First, eqn. (1) is a representation of conservation of mass inside the dendrite envelope, where the densities of the solid and liquid phases are assumed to be identical and constant, and the second identity in eqn. (1) simply states a growth kinetic law for a dendrite tip. It was derived from the Lipton, Glicksman and Kurz model [26], which is valid for both columnar and equiaxed growth in the case where only solutal undercooling is important and thermal and curvature undercoolings are negligible. Here Ω is the mean solutal supersaturation in the extradendritic liquid and $\mathrm{Iv}^{-1}(\Omega)$ stands for the inverse function of the Ivantsov function $\mathrm{Iv}(\mathrm{Pe}_\mathrm{t})$. Second, eqn (2) states that the increase in mass of the solute in the solid during $\mathrm{d}t$ results from the combined contributions of movement of the solid–liquid interface and solute diffusion across the interface. For negligible back diffusion in the solid, the last term on the right-hand side of eqn. (2) vanishes. Similarly, each term on the right-hand side of eqn. (3) represents a contribution to the change in mass of the solute in the interdendritic liquid; they are due to solid–interdendritic liquid interfacial movement (phase change), dendrite envelope growth, and solute diffusion across the two interfaces. Finally, eqn. (4) is a mathematical statement of the solute balance in phase l. Therefore, mathematically these equations represent an integral analysis of solute diffusion. This type of analysis avoids solving partial differential equations, but produces reasonably good approximations. The integral method has been applied successfully to a diverse variety of scientific and engineering problems (for example see ref. 27 for phase change problems).

The present solute diffusion model, consisting of eqns. (1)–(4), can readily be incorporated into a macroscopic heat flow model. In the absence of fluid flow, this is achieved mainly through the coupling

between the temperature field obtained from a macroscopic model and the solid fraction (and hence latent heat) evolution predicted from the present solute diffusion model; more details are provided in ref. 25. Furthermore, eqns. (1)–(4) are equally applicable to columnar and equiaxed dendritic growth, while leaving descriptions of the different physical characteristics of each mode of solidification to supplementary relations for S and l (see below). Lastly, it can be seen that the sum of eqns. (1)–(4) leads to the overall solute balance:

$$\frac{\mathrm{d}(\varepsilon_s\langle C_s\rangle^s)}{\mathrm{d}t}+\frac{\mathrm{d}(\varepsilon_d\bar{C}_e)}{\mathrm{d}t}+\frac{\mathrm{d}(\varepsilon_l\langle C_l\rangle^l)}{\mathrm{d}t}=0 \tag{6}$$

Integration gives

$$\varepsilon_s\langle C_s\rangle^s+\varepsilon_d\bar{C}_e+\varepsilon_l\langle C_l\rangle^l=C_o \tag{7}$$

After substituting $\bar{C}_{sd}$ by $\bar{C}_e$ using eqn. (5), eqns. (1)–(4) contain five unknowns: ε_s, ε_d, $\langle C_s\rangle^s$, $\bar{C}_e$ and $\langle C_l\rangle^l$. Supplied with one additional equation, which is referred to as the characteristic solidification equation as described in the next subsection, the present model is complete. The supplementary relations for the interfacial area concentrations, diffusion lengths and Ivantsov function are discussed in detail in Section 2.3.

2.2. Characteristic solidification equation

Various characteristic solidification equations are possible depending on the actual system under consideration and the simplifications made in its analysis. For instance, many models assume that the isothermal system is characterized by either a parabolic solidification rate, namely

$$\varepsilon_s\frac{\mathrm{d}\varepsilon_s}{\mathrm{d}t}=\frac{1}{2t_f} \tag{8}$$

or a constant cooling rate, *i.e.*

$$-\frac{\mathrm{d}T}{\mathrm{d}t}=-m_l\frac{\mathrm{d}\bar{C}_e}{\mathrm{d}t}=\dot{T} \tag{9}$$

where t_f is the final solidification time, $\dot{T}$ the cooling rate and m_l the slope of the liquidus line. Another typical characteristic solidification equation is the energy equation for an isothermal system, *i.e.*

$$q_{ext}A=V\left(\Delta h\frac{\mathrm{d}\varepsilon_s}{\mathrm{d}t}+c_p\frac{\mathrm{d}T}{\mathrm{d}t}\right) \tag{10}$$

where q_{ext} is the external heat extraction rate, and A and V are the surface area and volume of the system respectively. The terms Δh and c_p stand for the volumetric latent and specific heats respectively. With $q_{ext}A/V=c_p\dot{T}$, the above equation can be rewritten as

$$\dot{T}=\frac{\Delta h}{c_p}\frac{\mathrm{d}\varepsilon_s}{\mathrm{d}t}+m_l\frac{\mathrm{d}\bar{C}_e}{\mathrm{d}t} \tag{11}$$

The above three characteristic solidification equations, eqns. (8), (9) and (11), are employed in the following, depending on the system considered.

2.3. Supplementary relations

The supplementary relations needed for eqns. (1)–(4) are the Ivantsov function, the interfacial area concentrations and the diffusion lengths.

The growth kinetic law for a dendrite tip largely depends on the geometrical approximation made for the tip. By assuming a hemispherical dendrite tip, a linear $\mathrm{Iv}(\mathrm{Pe}_t)$ function results [4], thus

$$\mathrm{Iv}^{-1}(\Omega)=\Omega \tag{12}$$

and eqn. (1) reduces to a simple quadratic relation

$$\bar{w}_{ne}=\frac{D_l m_l(\kappa-1)\bar{C}_e}{\pi^2\Gamma}\Omega^2 \tag{13}$$

However, by assuming more realistically that the dendrite tip is a paraboloid of revolution, a complicated Ivantsov transport function $\mathrm{Iv}(\mathrm{Pe}_t)$ results whose evaluation involves an infinite series [4]. Finding the inverse of this function is apparently of high computational cost. Several approximations to $\mathrm{Iv}(\mathrm{Pe}_t)$ have been attempted in ref. 4, which are the so-called zeroth-, first- and second-order approximations. The growth equation for a hemispherical tip turns out to be the zeroth-order approximation for a parabolic tip. A comparison of all these approximations with the exact Ivantsov function is shown in Fig. 2. It can be seen

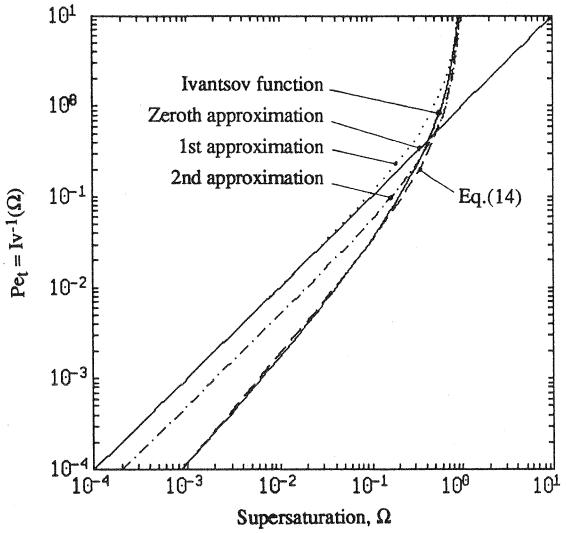

Fig. 2. Various approximations to the inverse Ivantsov function, $\mathrm{Pe}_t=\mathrm{Iv}^{-1}(\Omega)$. A new correlation, eqn. (14), gives the best agreement.

none of the approximations are satisfactory for implementation in a numerical model. Therefore, a new simple correlation is proposed to approximate the inverse Ivantsov function, which is

$$\mathrm{Pe}_t = \mathrm{Iv}^{-1}(\Omega) = a\left(\frac{\Omega}{1-\Omega}\right)^b \tag{14}$$

where $a = 0.4567$ and $b = 1.195$ give the best fit. The excellent agreement of this correlation with the exact Ivantsov function can be seen in Fig. 2. Therefore, eqn. (14) is used in all calculations presented in this paper.

Expressions for the interfacial area concentrations and the diffusion lengths were derived in ref. 25 and are summarized in Table 1. They are based on approximations of the dendrite geometry and formal microscopic analyses of the solute diffusion within each phase. The shape factor ϕ_e for the dendrite envelope is introduced to account for the deviation of the actual envelope shape from a sphere in the equiaxed case and from a cylinder in the columnar case. It is worth mentioning that Rappaz and Thevoz [23, 24] assume a spherical envelope. This is equivalent to a shape factor of unity. It is suggested in ref. 28 that typical values of ϕ_e range from 0.75 to unity. An investigation of the effect of the shape factor is conducted later. As can be seen from Table 1, a significant feature of the geometrical relations is that they directly invoke key metallurgical parameters, such as the primary arm spacing, the nuclei density and the secondary arm spacing. Alternatively, one could derive expressions directly for (and measure) the interfacial area concentrations [29]. It is also noticed that the final equivalent radius of an equiaxed grain R_f is obtained from the nuclei density, where it is implied that nucleation occurs at a single temperature. Incorporation of other more sophisticated nucleation laws [1] is straightforward.

The expression for the solid diffusion length, as listed in Table 1, was obtained by assuming a parabolic concentration profile in the solid (as in ref. 7), while those for l_{ld} were derived by invoking the quasi-steady assumption and analytically solving the one-dimensional solute diffusion equation in the extradendritic liquid.

2.4. Initial conditions

The appropriate initial conditions are, when $t = 0$,

$$\begin{aligned} &\varepsilon_s = \varepsilon_d = 0 \\ &\langle C_s \rangle^s = \kappa \bar{C}_e \\ &\bar{C}_e = C_o - \frac{\Delta T}{m_l} \\ &\langle C_l \rangle^l = C_o \end{aligned} \tag{15}$$

where ΔT is either the nucleation undercooling, ΔT_N in equiaxed growth or the initial tip undercooling ΔT_c at the columnar front. Generally, ΔT_N is specified by a

TABLE 1. Summary of the supplementary relations for equiaxed and columnar systems

Quantity	Equiaxed growth	Columnar growth
Final radius of dendrite R_f	$\left(\frac{4}{3}\pi n\right)^{-1/3}$	$\lambda_1/\pi^{1/2}$
Solid–interdendritic liquid interfacial area concentration S_s	$2/\lambda_2$	$2/\lambda_2$
Envelope area concentration S_e	$\frac{3(\varepsilon_s+\varepsilon_d)^{2/3}}{R_f\phi_e}$	$\frac{2(\varepsilon_s+\varepsilon_d)^{1/2}}{R_f\phi_e}$
Solid diffusion length l_{sd}	$\frac{\varepsilon_s\lambda_2}{6(1-\varepsilon_l)}$	$\frac{\varepsilon_s\lambda_2}{6(1-\varepsilon_l)}$
Liquid diffusion length l_{ld}	$l_{ld}/R_f = \frac{1}{\mathrm{Pe}}\left\{1-\frac{3}{\varepsilon_l}\exp[-\mathrm{Pe}(1-\varepsilon_l)^{1/3}] \times \int_{(1-\varepsilon_l)^{1/3}}^{1} x^2 \exp\left[\frac{\mathrm{Pe}(1-\varepsilon_l)^{2/3}}{x}\right] dx\right\}$ (spherical model) $\mathrm{Pe} = \bar{w}_{ne}R_f/D_l$	$l_{ld}/R_f = \frac{1}{\mathrm{Pe}}\left\{1-\frac{2}{\varepsilon_l}\exp\left[\frac{\mathrm{Pe}}{2}(1-\varepsilon_l)^{1/2}\ln(1-\varepsilon_l)\right] \times \int_{(1-\varepsilon_l)^{1/2}}^{1} x\exp[-\mathrm{Pe}(1-\varepsilon_l)^{1/2}\ln x]\,dx\right\}$ (cylindrical model) $\mathrm{Pe} = \bar{w}_{ne}R_f/D_l$

nucleation law, whereas ΔT_c can be determined from the initial tip growth velocity using the growth kinetic relation as given above.

2.5. Numerical procedures

Equations (1)-(4) and one of eqns. (8), (9) and (11) subject to the initial conditions, eqn. (15), are not amenable to analytical solution. Therefore, a numerical procedure is employed which consists of the standard fourth-order Runge-Kutta method for the set of ordinary differential equations and the 21-point Gauss-Kronrod rule for numerical integration of the liquid diffusion length. In some extreme cases (*e.g.* high cooling rates and/or large growth velocities), the present solute diffusion model becomes a stiff problem, thus requiring the Gear method in place of the Runge-Kutta method. All subroutines of relevance are available in the IMSL Mathematical Library [30].

3. Results and discussion

In this section, various applications of the present unified solute diffusion model for columnar and equiaxed dendritic growth are illustrated. Results are presented first for the case of equilibrium growth (*i.e.* without undercooling) and then for columnar and equiaxed solidification with tip undercooling.

3.1. Complete solute mixing in the liquid

By neglecting dendrite tip undercooling, *i.e.* assuming complete solute mixing in the interdendritic and extradendritic liquid, the overall solute balance, eqn. (6), reduces to

$$\frac{\mathrm{d}(\varepsilon_s\langle C_s\rangle^s)}{\mathrm{d}t}+\frac{\mathrm{d}[(1-\varepsilon_s)\,\bar{C}_e]}{\mathrm{d}t}=0 \tag{16}$$

or in integrated form

$$\varepsilon_s\langle C_s\rangle^s+(1-\varepsilon_s)\,\bar{C}_e=C_o \tag{17}$$

In this case, the model reduces to a set of only three equations: eqns. (2), (17) and one characteristic solidification equation. It is shown below that this type of analysis can produce simple results for microsegregation which are of considerable accuracy.

Restricting further attention to a parabolic solidification rate, eqn. (8) is chosen as the proper characteristic solidification equation. Rewriting eqn. (2) and changing the coordinate from t to ε_s with the help of eqn. (8), yields

$$\varepsilon_s\frac{\mathrm{d}\langle C_s\rangle^s}{\mathrm{d}\varepsilon_s}=(1+6\alpha)(\kappa\bar{C}_e-\langle C_s\rangle^s) \tag{18}$$

where use has been made of the relations $S_s=2/\lambda_2$ and $l_{sd}=\varepsilon_s\lambda_2/6$ as given in Table 1 for both columnar and equiaxed growth. The parameter α is the traditional diffusion Fourier number based on the secondary dendrite arm spacing, which represents the extent of solute diffusion in the solid; it is defined as

$$\alpha=\frac{4D_s t_f}{\lambda_2^{\,2}} \tag{19}$$

Further substituting $\bar{C}_e$ for $\langle C_s\rangle^s$ in recognition of eqn. (17), one arrives at the following first-order differential equation for $\bar{C}_e$:

$$\frac{\mathrm{d}\bar{C}_e}{\mathrm{d}\varepsilon_s}+\left[\frac{(1+6\alpha)\kappa-1}{1-\varepsilon_s}+\frac{6\alpha}{\varepsilon_s}\right]\bar{C}_e=\frac{6\alpha}{\varepsilon_s(1-\varepsilon_s)}\,C_o \tag{20}$$

When $\alpha\to\infty$, eqn. (20) reduces to an algebraic equation from which the Lever rule is recovered:

$$\frac{\bar{C}_e}{C_o}=\frac{1}{1-(1-\kappa)\,\varepsilon_s} \tag{21}$$

In the other limit, $\alpha=0$, eqn. (20) admits a simple solution:

$$\frac{\bar{C}_e}{C_o}=(1-\varepsilon_s)^{\kappa-1} \tag{22}$$

which is known as the Scheil equation. For $\alpha\neq 0$, eqn. (20) also has a closed-form analytical solution:

$$\frac{\bar{C}_e}{C_o}=\frac{6\alpha(1-\varepsilon_s)^{(1+6\alpha)\kappa-1}}{\varepsilon_s^{\,6\alpha}}\int_0^{\varepsilon_s}\varepsilon^{6\alpha-1}(1-\varepsilon)^{-(1+6\alpha)\kappa}\,\mathrm{d}\varepsilon \tag{23}$$

The above expression represents an exact solution to the integral formulation of the solute redistribution problem, without invoking additional approximations. While Ohnaka's analysis [7] is also based on the integral method, his analytical result for $\bar{C}_e/C_o$ was obtained with the help of an additional approximation, which is $\mathrm{d}c/\mathrm{d}t\approx 0$. In terms of the present terminology, this assumption is equivalent to the following [7]:

$$\frac{\mathrm{d}}{\mathrm{d}t}\left(\frac{\bar{C}_{sd}-\langle C_s\rangle^s}{\varepsilon_s^{\,2}}\right)\approx 0 \tag{24}$$

It is easy to show that eqn. (18) combined with eqn. (24) indeed results in Ohnaka's solution:

$$\frac{\bar{C}_e}{C_o}=(1-\gamma\varepsilon_s)^{(\kappa-1)/\gamma} \tag{25}$$

where

$$\gamma=1-\frac{2\alpha\kappa}{1+2\alpha} \tag{26}$$

Figure 3 compares microsegregation of P in δ-Fe as predicted by various solute diffusion models. In particular, the present solution, eqn. (23), and Ohnaka's result, eqns. (25) and (26), are compared with Kobayashi's exact solution [8]. Apparently, the additional assumption, eqn. (24), results in a considerable loss of accuracy. Also, the present result is the most accurate of the analytical solutions.

In cases where a parabolic solidification rate cannot be assumed, the present model requires the solution of only one ordinary differential equation, eqn. (2), together with the characteristic solidification equation and an algebraic equation, eqn. (17). In contrast to purely numerical approaches [2, 3, 9–11], the present model avoids the complication of tracking a moving boundary, thus greatly alleviating solution efforts. However, the present analysis retains all the flexibility that a numerical model can have. For example, cases with variable partition and mass diffusion coefficients can be handled, and various characteristic solidification equations can be used.

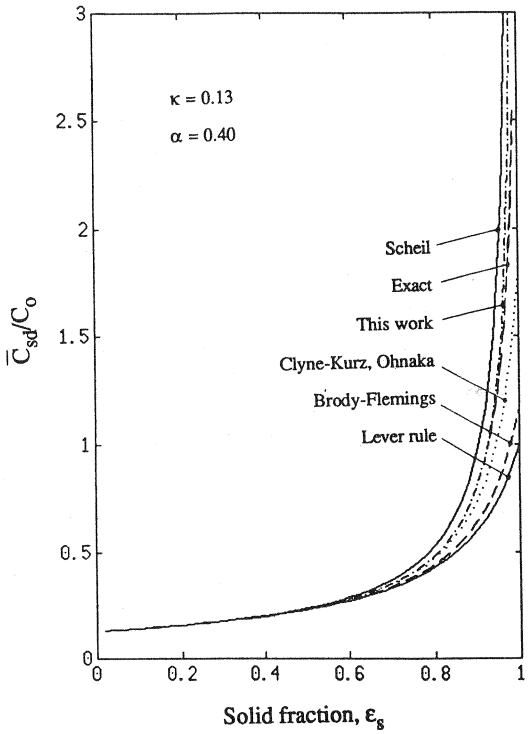

Fig. 3. Microsegregation of P in δ-Fe, as predicted by various solute diffusion models.

3.2. *Columnar growth with dendrite tip undercooling*

At intermediate and high cooling rates, diffusion in the solid is found to be negligible. However, another effect begins to influence the relation between the solid fraction and temperature: the dendrite tip temperature falls significantly below the equilibrium liquidus temperature. Some recent theoretical studies of the tip undercooling effect have been reported by Giovanola and Kurz [14] for an Ag–Cu alloy and by Flemings [31] for an Al–Cu alloy. Both studies are based on the "patching" method due to Giovanola and Kurz [14].

Numerical simulations based on the present model, eqns. (1)–(4), together with a constant cooling rate as the characteristic solidification equation, have been performed for an Al–4.5wt.%Cu alloy. The physical properties used for the results presented here are listed in Table 2. Besides the cooling rate and the undercooling prevailing around the primary dendrite tips (or the growth velocity), the dendrite arm spacings are also necessary inputs to the present model. These parameters can be estimated from the cooling rate, growth velocity and temperature gradient via certain empirical or theoretical relations available in the literature [4]. For example, Jones [32] shows that the secondary arm spacing can be correlated as a function of the cooling rate:

$$\lambda_2 = 50\,\dot{T}^{-1/3} \tag{27}$$

where λ_2 is the secondary arm spacing (in micrometers) and $\dot{T}$ is the cooling rate (in degrees kelvin per second). The equation was obtained by correlating data from a wide range of investigations for Al–(4–5)wt.%Cu and Al–(7–10)wt.%Si alloys. The primary arm spacing can

TABLE 2. Physical properties of various alloys used in the calculations

Quantity	Symbol	Al–Cu [2]	Ag–Cu [15]	Al–Si [23]	Unit
Eutectic concentration	C_E	33.2	—	10.77	wt.%
Volumetric specific heat	c_p	3.4×10^6	—	2.35×10^6	$J\,m^{-3}\,K^{-1}$
Diffusion coefficient	D_l	5.0×10^{-9}	2.0×10^{-9}	3.0×10^{-9}	$m^2\,s^{-1}$
	D_s	5.0×10^{-13}	—	—	$m^2\,s^{-1}$
Gibbs–Thomson coefficient	Γ	2.41×10^{-7}	1.53×10^{-7}	0.9×10^{-7}	mK
Partition coefficient	κ	0.17	0.41	0.117	wt.% per wt.%
Volumetric latent heat	Δh	1.02×10^9	—	9.5×10^8	$J\,m^{-3}$
Liquidus slope	m_l	−3.37	−6.46	−7.7	K wt.%$^{-1}$
Melting point of pure metal	T_m	933	—	933	K

be predicted from the theory developed by Hunt [33]:

$$\lambda_1 = [64\Gamma D_l m_l (1-\kappa) C_o]^{1/4} G^{-1/2} V_t^{-1/4} \quad (28)$$

The other theory due to Kurz and Fisher [34] basically has the same form except for a different numerical constant. Noting that the temperature gradient G is equal to $\dot{T}/V_t$, eqn. (28) can be rewritten as

$$\lambda_1 = [64\Gamma D_l m_l (1-\kappa) C_o]^{1/4} \dot{T}^{-1/2} V_t^{1/4} \quad (29)$$

for convenient use in the present numerical simulations.

To examine the sole effect of dendrite tip undercooling, calculations are carried out for two cooling rates $\dot{T} = 10^3$ and 10^6 K s^{-1} and by setting $D_s = 0$ in the model equations. The predicted temperature *vs.* solid fraction curves are plotted in Fig. 4 together with Flemings' results. It can be seen that the two predictions basically produce the same trend. The temperature undergoes little change during the initial long stage of solidification, and only decreases significantly during the last short period of solidification. The other consequence of dendrite tip undercooling is a decrease in the fraction of eutectic. It should be realized that, in contrast to the patching method of Giovanola and Kurz [14], a single set of equations is used in the present model throughout the entire mushy region. By adding up eqns. (3) and (4), transforming the coordinate from t to ε_s and making some rearrangements, one arrives at

$$(1-\varepsilon_s)\frac{d\bar{C}_e}{d\varepsilon_s} + (\kappa-1)\bar{C}_e = \frac{d}{d\varepsilon_s}[\varepsilon_l(\bar{C}_e - \langle C_l \rangle^l)] \quad (30)$$

where the interfacial terms have been cancelled out and diffusion in the solid is neglected (*i.e.* $D_s = 0$). It is now clear that, as the solidification path asymptotically reaches a state of complete solute mixing in the liquid, the right-hand side of eqn. (30) vanishes, and the present model automatically reduces to the Scheil equation (recall that $\bar{C}_e$ is equal to the liquid concentration at the solid–liquid interface).

Another numerical study using the present model is conducted for an Ag–15wt.%Cu alloy, again assuming negligible back diffusion in the solid. Calculations are carried out using the physical properties listed in Table 2, a tip growth velocity of 12 cm s^{-1}, and a primary dendrite arm spacing of 0.3 μm. These data are taken directly from the experiment of Bendersky and Boettinger [35]. The predicted microsegregation profile is plotted in Fig. 5, together with Giovanola and Kurz's result as well as the experimental data measured by Bendersky and Boettinger [35]. It can be seen that all three results are in good agreement, thus validating the present model in accounting for the influence of dendrite tip undercooling. Slight differences between the present results and those from the Giovanola and Kurz model can be observed in both Figs. 4 and 5. They can be attributed to the simplified treatment of the dendrite morphology in Giovanola and Kurz' patching method [14]. In fact, it can be argued that the present predictions in Fig. 5 are in somewhat better agreement with the experimental data.

In order to predict microsegregation over a wide range of cooling rates, however, the effects of back dif-

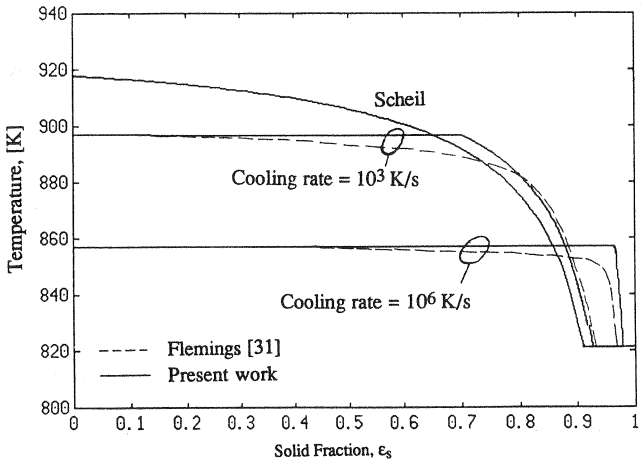

Fig. 4. Effect of dendrite tip undercooling on the temperature *vs.* solid fraction relation for columnar solidification of an Al–4.5wt.%Cu alloy.

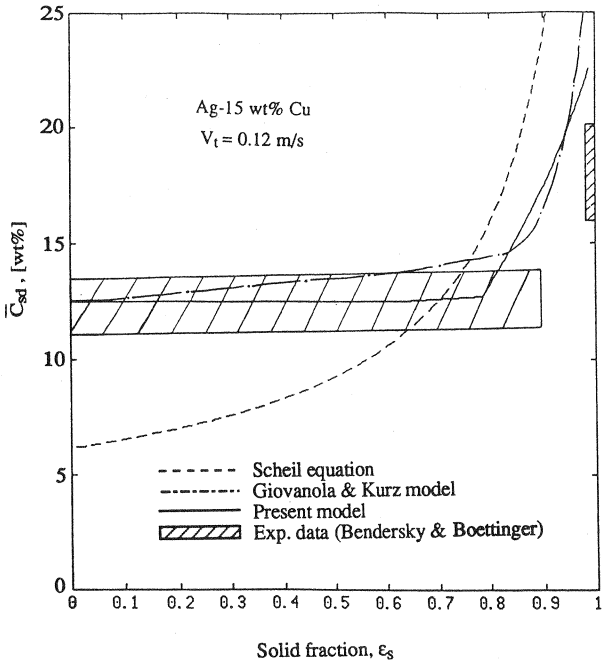

Fig. 5. Comparisons of the present prediction of microsegregation in a rapidly solidified Ag–15wt.%Cu alloy with Giovanola and Kurz's calculation [14] and the experimental data of Bendersky and Boettinger [35].

TABLE 3. Comparison of the present theoretical predictions of the eutectic fraction with the measurements of Sarreal and Abbaschian [21] for an Al–4.9wt.%Cu alloy (the measured values correspond to mass fractions as calculated in ref. 3)

Run number	Cooling rate ($K\ s^{-1}$)	Growth velocity ($m\ s^{-1}$)	Eutectic fraction (%) measured	Eutectic fraction (%) predicted	Relative error (%)
1	0.1	10^{-5}	6.61	6.15	−6.96
2	1.05	10^{-4}	7.74	8.22	6.20
3	11.25	1.5×10^{-3}	8.40	9.12	8.57
4	65	5.0×10^{-3}	8.81	9.30	5.56
5	187	10^{-2}	9.25	9.41	1.73
6	1700	10^{-1}	7.56	8.43	11.5

fusion in the solid and dendrite tip undercooling need to be taken into account simultaneously. Recently, Sarreal and Abbaschian [21] presented a set of experimental data for an Al–4.9wt.%Cu alloy in order to demonstrate the influence of the cooling rate on microsegregation. Interestingly, they found that the eutectic fraction first increases as the cooling rate rises up to 187 $K\ s^{-1}$ and then decreases with increasing cooling rate. This behavior cannot be captured by a solute diffusion model that considers either solid diffusion only or dendrite tip undercooling alone, as indicated in ref. 2. Since the present model includes both these factors, it can be expected to be an appropriate theoretical tool for explaining the experimental observation. Several numerical simulations are performed for solidification for an Al–4.9wt.%Cu alloy at the cooling rates and growth velocities of the experiments. In the calculations, eutectic undercooling is neglected and constant alloy properties are assumed. The predictions of the eutectic fraction are tabulated in Table 3 together with the experimental data of Sarreal and Abbaschian [21], where the experimental values correspond to the mass fraction of eutectic as calculated in ref. 3. It is found that the agreement between the present predictions and the experimental results is fairly good, with the relative error ranging from 1.73% to 11.5%. By including eutectic undercooling and variable alloy properties, Roosz and Exner [19] and Voller and Sundarraj [20] obtained even better agreement. Nonetheless, the important fact that the eutectic fraction is reduced at a very high cooling rate (run number 6) is predicted by the present model. This is known to be due to the effect of dendrite tip undercooling on microsegregation. Figure 6 shows the effect of the cooling rate on the normalized eutectic fraction $\varepsilon_E/\varepsilon_{Emax}$, where ε_{Emax} is the value computed from the Scheil equation and also represents the theoretical maximum eutectic fraction. It can be seen that the eutectic fraction is always below the Scheil value. At low cooling rates back diffusion in the solid causes a reduction in the eutectic fraction, while at high rates dendrite tip undercooling tends to decrease the eutectic fraction. However, the two effects are not additive. At low cooling rates the effect of dendrite tip undercooling does not exist, while at very high cooling rates diffusion in the solid phase becomes negligible owing to the short duration of the solidification process.

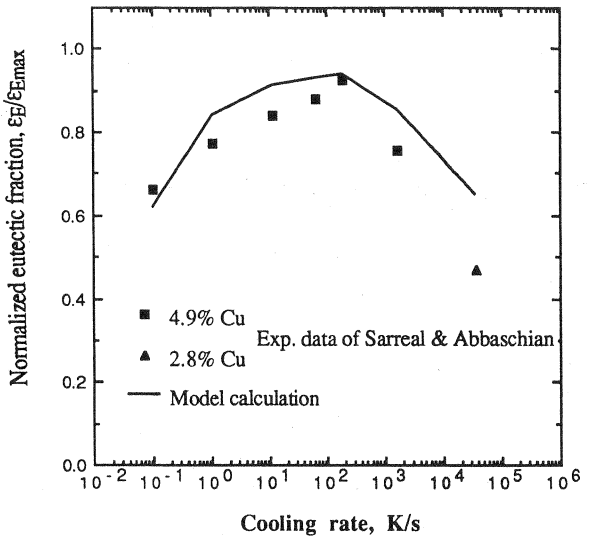

Fig. 6. Effect of cooling rate on the eutectic fraction. Comparison of the present predictions with Sarreal and Abbaschian's experiments [21].

3.3. *Equiaxed growth*

For equiaxed dendritic solidification, the same set of equations is employed and solved, except for the appropriate supplementary relations as listed in Table 1. Equation (11), which represents the heat balance of an isothermal system, is used as the characteristic solidification equation for all results presented in this subsection.

In order to validate the present model for equiaxed dendritic growth, solidification of an Al–5wt.%Si alloy, whose physical properties are listed in Table 2, is simulated. A series of predicted cooling curves for a

cooling rate of 45 K s^{-1} and three different final grain radii is first compared against the more exact solution due to Rappaz and Thevoz [23], as shown in Fig. 7. The latter was obtained by solving a microscopic partial differential equation for solute diffusion in the extradendritic liquid by a finite difference technique and was based on the quadratic growth law, eqn. (13). It can be seen that excellent agreement between the two predictions exists, although the present model utilizes the simpler concept of a diffusion length together with an integral formulation. To investigate the effect of the liquid diffusion length, a series of preliminary calculations using different diffusion lengths has been performed. As pointed out in ref. 25, a physically meaningful diffusion length should satisfy the following constraint:

$$l_{ld} \leq \frac{D_l}{w_{ne}} \tag{31}$$

under which $d\langle C_l\rangle^l/dt$ is greater than zero. The equality holds when $d\langle C_l\rangle^l/dt = 0$ (see eqn. (4)), *i.e.* the average concentration in the extradendritic liquid $\langle C_l\rangle^l$ always remains at the initial composition C_0. This is the key assumption made in the analytical model of Rappaz and Thevoz [24]. However, the assumption leads to a failure to arrive at a state of complete solute mixing in the liquid during the later stages of solidification. As a remedy, Rappaz and Thevoz [24] implement a certain correction procedure to ensure a smooth transition to the state of complete solute mixing. In contrast, the present expression for the diffusion length given in Table 1 satisfies the above constraint, and the solution of eqn. (4) provides the time evolution of the average concentration in the extradendritic liquid $\langle C_l\rangle^l$.

Another approximate diffusion length can be obtained by expressing the exponential function in the integrand of the quasi-steady solution in Table 1 by a series expansion. Choosing the first three terms only, the integral becomes

$$\text{Integral} = \frac{\varepsilon_L}{3}\left[1 + \frac{3}{2}(1-\varepsilon_l)^{2/3} \times \text{Pe}\,\frac{1+(1-\varepsilon_l)^{1/3}+(1-\varepsilon_l)^{2/3}\text{Pe}}{1+1-\varepsilon_l^{1/3}+(1-\varepsilon_l)^{2/3}}\right] \tag{32}$$

It should be noted that the diffusion length with the integral evaluated by eqn. (32) also satisfies the constraint given by eqn. (31). A comparison has been made (not reported here for brevity) of the predicted cooling curves using Rappaz and Thevoz's expression for the diffusion length (*i.e.* the equality in eqn. (31)), the approximate expression given by eqn. (32), and the general expression given in Table 1. It is found that the model is relatively insensitive to the choice of liquid diffusion length. This helps to clarify the fact that the present model and the analytical model of Rappaz and Thevoz [24] can yield reasonably accurate results for the cooling curves.

As shown in Fig. 8, there is, however, a relatively large discrepancy in the predictions of the grain frac-

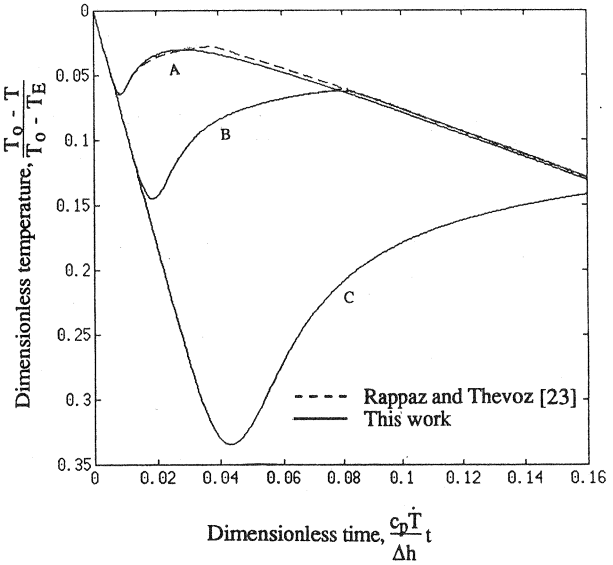

Fig. 7. Comparisons of cooling curves for equiaxed dendritic growth, as predicted by the present model (——) and Rappaz and Thevoz [23] (– – –) for final grain radii of (A) 100 μm, (B) 1 mm and (C) 10 mm.

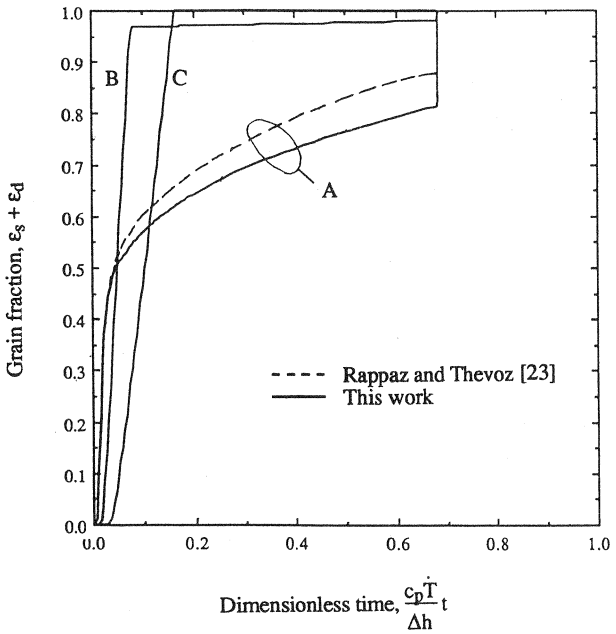

Fig. 8. Comparisons of the grain fraction for equiaxed dendritic growth, as predicted by the present model (——) and Rappaz and Thevoz [23] (– – –) for final grain radii of (A) 100 μm, (B) 1 mm and (C) 10 mm.

tion ($\varepsilon_s + \varepsilon_d = 1 - \varepsilon_l$) from the two models in the case of $R_f = 100$ μm. The reason lies in a subtle difference in the growth kinetics model for the dendrite tips. The present model considers the driving force for the envelope growth to be ($\bar{C}_e - \langle C_l \rangle^l$), the difference between the concentration at the envelope (*i.e.* the tips) and the average concentration in the extradendritic liquid. However, Rappaz and Thevoz use ($\bar{C}_e - C_R$), where C_R is the minimum liquid concentration located at the outer boundary of the grain. The driving force in Rappaz and Thevoz's model allows for a larger growth velocity and consequently a higher grain fraction, because $\langle C_l \rangle^l$ is always higher than C_R. This factor is important in the case of $R_f = 100$ μm. In contrast, in the other two cases (*i.e.* $R_f = 1$ and 10 mm), the grain growth is so fast that $\langle C_l \rangle^l$ does not deviate much from C_R throughout the grain growth period (*i.e.* $\langle C_l \rangle^l \approx C_R \approx C_o$). Hence, virtually no difference between the two predictions is observed. It is worth mentioning that Kanetkar and Stefanescu [36] also use the term ($\bar{C}_e - \langle C_l \rangle^l$) as the driving force for dendrite tip growth in their solidification kinetics-heat transfer model.

Figure 8 also provides quantitative information about the distribution of the eutectic phase in the interdendritic and extradendritic regions. For instance, in the case of $R_f = 100$ μm, the total eutectic fraction is equal to 0.4, while the fraction of the eutectic phase between the grains amounts to 0.18. Accordingly, the fractions of the eutectic phase in the interdendritic and extradendritic regions are 0.22 and 0.18 respectively. Validation of the above predictions of the grain fraction evolution and the eutectic fractions is not possible at the present time owing to a lack of suitable experimental data.

In comparing their model predictions to experimental data, Rappaz and Thevoz [23] questioned two assumptions underlying their model: the quadratic growth law and the assumed spherical shape of the dendrite envelope. The validity of both approximations can be examined qualitatively using the present solute diffusion model. Figure 9 shows a comparison of cooling curves obtained using the quadratic relation, eqn. (13), as well as the more exact growth law based on the Ivantsov function, eqn. (14). As expected, the depth of recalescence is larger for all three radii when using the growth kinetic law for a parabolic tip. Hence, the use of an improved growth law may lead to a better agreement between experiment and theory.

However, the assumption of a spherical dendrite envelope does not appreciably deteriorate the predictions of recalescence. As shown in Fig. 10, the adoption of a non-spherical envelope with a shape factor ("sphericity") of 0.8 brings about no significant difference compared with the case of a spherical envelope.

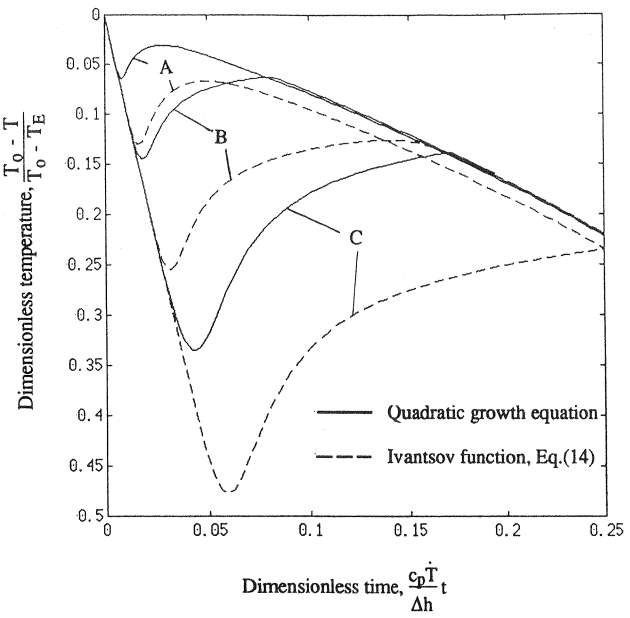

Fig. 9. Effect of the growth kinetic law on the predicted recalescence for final grain radii of (A) 100 μm, (B) 1 mm and (C) 10 mm.

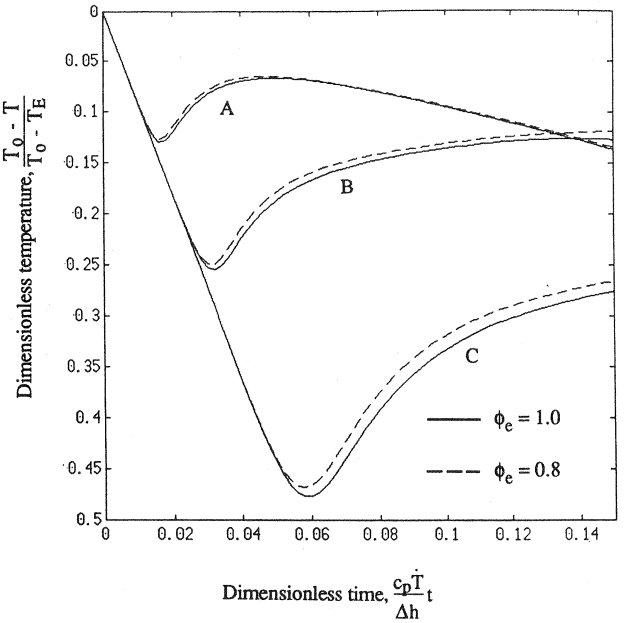

Fig. 10. Influence of a non-spherical dendrite envelope on the predicted recalescence for final grain radii of (A) 100 μm, (B) 1 mm and (C) 10 mm.

4. Conclusions

(1) A unified solute diffusion model for columnar and equiaxed dendritic solidification is presented. Mathematically, the model is rigorously derived using the volume averaging technique and a multiphase approach. Physically, the model represents an integral

analysis, so that solute is conserved both locally within each phase and overall for all phases.

(2) The model gives an adequate description of crystal growth, by including basic microscopic phenomena such as nucleation, back diffusion in the solid, growth kinetics of the dendrite tip, and dendrite morphology.

(3) In accounting for back diffusion in the solid alone, the paper develops a closed-form exact solution to the integral formulation of the solute redistribution problem. The solution significantly improves Ohnaka's analytical result and agrees well with the exact solution due to Kobayashi for microsegregation of P in δ-Fe.

(4) Regarding the effect of dendrite tip undercooling in columnar growth alone, the model predictions are in agreement with those from the Giovanola and Kurz patching method, as shown for Al–4.5wt.%Cu and Ag–15wt.%Cu alloys. Also, the present predictions agree with Bendersky and Boettinger's experiments for an Ag–15wt.%Cu alloy.

(5) For the purpose of predicting microsegregation, the model can reflect the influences of both solid diffusion and dendrite tip undercooling. The theoretical predictions for columnar dendritic solidification of an Al–4.9wt.%Cu alloy are in good agreement with experimental data for a wide range of cooling rates.

(6) For equiaxed dendritic growth, the model successfully predicts recalescence and the distribution of the eutectic phase in the interdendritic and extradendritic regions. The example calculations are in excellent agreement with the more exact solutions of Rappaz and Thevoz using a finite difference method. In addition, the assumptions of a quadratic growth law and a spherical dendrite envelope are examined.

(7) The present model provides a useful alternative to current solute diffusion models for use in macroscopic heat transfer codes. In addition to growth kinetics, it also incorporates back diffusion in the solid and allows for the prediction of microsegregation over a wide range of cooling rates. The model is equally valid for columnar and equiaxed dendritic growth. Therefore, efforts are under way to apply the model to mixed columnar and equiaxed solidification of alloys.

Acknowledgments

This work was supported by the National Science Foundation under Grant No. CTS-8957149 and by the ALCOA Technical Center, Alcoa Center, PA.

References

1 M. Rappaz, *Int. Mater. Rev., 34* (1989) 93–123.
2 T. P. Battle and R. D. Pehlke, *Metall. Trans. B, 21* (1990) 357–375.
3 S. Sundarraj and V. R. Voller, in C. Beckermann, L. A. Bertram, S. J. Pien and R. E. Smelser (eds.), *Micro/Macro Scale Phenomena in Solidification*, ASME publication, HTD-218, ASME, New York, 1992, pp. 35–42.
4 W. Kurz and D. J. Fisher, *Fundamentals of Solidification*, Trans. Tech. Publications, Aedermannsdorf, 1989.
5 H. D. Brody and M. C. Flemings, *Trans. AIME, 236* (1966) 615–624.
6 T. W. Clyne and W. Kurz, *Metall. Trans. A, 12* (1981) 965–971.
7 I. Ohnaka, *Trans. ISIJ, 26* (1986) 1045–1051.
8 S. Kobayashi, *J. Cryst. Growth, 88* (1988) 87–96.
9 A. J. W. Ogilvy and D. H. Kirkwood, *Appl. Sci. Res., 44* (1987) 43–49.
10 S. Sundarraj and V. R. Voller, *Int. J. Heat Mass Transfer, 36* (1993) 713–724.
11 K. S. Yeum, V. Laxmanan and D. P. Poirier, *Metall. Trans. A, 20* (1989) 2847–2856.
12 M. C. Flemings, in J. E. Lait and I. V. Samarasekera (eds.), *F. Weinberg Int. Conf. on Solidification Processing*, Pergamon, New York, 1990, pp. 173–194.
13 S. C. Flood and J. D. Hunt, *Appl. Sci. Res., 44* (1987) 27–42.
14 B. Giovanola and W. Kurz, *Metall. Trans. A, 21* (1990) 260–263.
15 W. Kurz, B. Giovanola and R. Trivedi, *Acta Metall., 34* (1986) 823–830.
16 M. Solari and H. Biloni, *J. Cryst. Growth, 49* (1980) 451–457.
17 M. H. Burden and J. D. Hunt, *J. Cryst. Growth, 22* (1974) 109–116.
18 H. E. Exner, A. Roosz and M. Rettenmayr, in M. Rappaz, M. R. Ozgu and K. W. Mahin (eds.), *Modeling of Casting, Welding and Advanced Solidification Processes V*, TMS, Warrendale, PA, 1991, pp. 429–434.
19 A. Roosz and H. E. Exner, in T. S. Piwonka, V. Voller and L. Katgerman (eds.), *Modeling of Casting, Welding and Advanced Solidification Processes VI*, TMS, Warrendale, PA, 1993, pp. 243–250.
20 V. R. Voller and S. Sundarraj, in T. S. Piwonka, V. Voller and L. Katgerman (eds.), *Modeling of Casting, Welding and Advanced Solidification Processes VI*, TMS, Warrendale, PA, 1993, pp. 251–258.
21 J. A. Sarreal and G. J. Abbaschian, *Metall. Trans. A, 17* (1986) 2063–2073.
22 J. Dustin and W. Kurz, *Z. Metallkd., 77* (1986) 265–273.
23 M. Rappaz and Ph. Thevoz, *Acta Metall., 35* (1987) 1487–1497.
24 M. Rappaz and Ph. Thevoz, *Acta Metall., 35* (1987) 2929–2933.
25 C. Y. Wang and C. Beckermann, in C. Beckermann, L. A. Bertram, S. J. Pien and R. E. Smelser (eds.), *Micro/Macro Scale Phenomena in Solidification*, ASME publication, HTD-218, ASME, New York, 1992, pp. 43–58; also *Metall. Trans. A*, in press.
26 J. Lipton, M. E. Glicksman and W. Kurz, *Mater. Sci. Eng., 65* (1984) 57–63.
27 T. R. Goodman, *Trans. ASME, 8* (1958) 335–342.
28 S. Ahuja and C. Beckermann, in C. Beckermann, L. A. Bertram, S. L. Pien and R. E. Smelser (eds.), *Micro/Macro Scale Phenomena in Solidification*, ASME publication, HTD-218, ASME, New York, 1992, pp. 85–91.
29 S. P. Marsh and M. E. Glicksman, in T. S. Piwonka, V. Voller and L. Katgerman (eds.), *Modeling of Casting, Welding and*

Advanced Solidification Processes VI, TMS, Warrendale, PA, 1993, pp. 55–62.
30 IMSL, International mathematical and statistical library manual, Houston, TX, 1984.
31 M. C. Flemings, *Metall. Trans. A, 22* (1991) 957–981.
32 H. Jones, *Mater. Sci. Eng., 65* (1984) 145–156.
33 J. D. Hunt, *Solidification and Casting of Metals*, Metal Society, London, 1979, pp. 3–9.
34 W. Kurz and D. J. Fisher, *Acta Metall., 29* (1981) 11–20.
35 L. A. Bendersky and W. J. Boettinger, in S. Warlimont (ed.), *Rapidly Quenched Metals*, Vol. 1, North-Holland, Amsterdam, 1985, pp. 887–890.
36 C. S. Kanetkar and D. M. Stefanescu, in A. F. Giamei and G. J. Abbaschian (eds.), *Modeling and Control of Casting and Welding Processes IV*, TMS, Warrendale, PA, 1988, pp. 697–708.

Appendix A: Nomenclature

a	coefficient in eqn. (14)
A	interfacial surface area
b	index in eqn. (14)
C	concentration of a chemical species
$\langle C_k \rangle^k$	mean concentration in phase k
$\bar{C}_{kj}$	interfacial concentration at the k–j interface
c_p	volumetric specific heat
D	mass diffusion coefficient
G	temperature gradient
Iv	Ivantsov function
l	solute diffusion length
m_l	liquidus line slope
n	equiaxed nuclei density
Pe	envelope Peclet number, $\mathrm{Pe} = \bar{w}_{ne} R_f / D_l$
Pe_t	tip Peclet number, $\mathrm{Pe}_t = V_t R_t / (2D_l)$
q_{ext}	external heat extraction rate
R	radius
S	interfacial area concentration
t	time
t_f	final solidification time
T	temperature
$\dot{T}$	cooling rate
V	volume
V_t	dendrite tip velocity
$\bar{w}_{ne}$	envelope velocity

Greek symbols

α	diffusion Fourier number as defined in eqn. (19)
γ	parameter defined in eqn. (26)
Γ	Gibbs–Thomson coefficient in the kinetic law for dendrite growth
Δh	latent heat of phase change
ΔT	undercooling
ε	volume fraction
κ	partition coefficient
λ_1	primary dendrite arm spacing
λ_2	secondary dendrite arm spacing
ϕ	shape factor
Ω	solutal supersaturation, $(\bar{C}_e - \langle C_l \rangle^l)/[\bar{C}_e(1-\kappa)]$

Subscripts

c	columnar front
d	interdendritic liquid
e	dendrite envelope
E	eutectic point
f	final dimension of the envelope
l	extradendritic liquid
ld	extradendritic–interdendritic liquid interface
m	melting point of pure metals
N	nucleation
o	initial state
R	outer boundary of equiaxed grain
s	solid
sd	solid–interdendritic liquid interface
t	dendrite tip